ESMC: MLLM-Based Embedding Selection for Explainable Multiple Clustering

Xinyue Wang[1], **Yuheng Jia**[1,2, 3*], **Hui Liu**[3], **Junhui Hou**[4]

[1]School of Computer Science and Engineering, Southeast University, Nanjing 210096, China
[2]Key Laboratory of New Generation Artificial Intelligence Technology and Its Interdisciplinary Applications
(Southeast University), Ministry of Education, China
[3]Department of Computing and Information Sciences, Saint Francis University, Hong Kong, China
[4]Department of Computer Science, City University of Hong Kong, Hong Kong, China
213222801@seu.edu.cn, yhjia@seu.edu.cn, h2liu@sfu.edu.hk, jh.hou@cityu.edu.hk

Abstract

Typical deep clustering methods, while achieving notable progress, can only provide one clustering result per dataset. This limitation arises from their assumption of a fixed underlying data distribution, which may fail to meet user needs and provide unsatisfactory clustering outcomes. Our work investigates how multi-modal large language models (MLLMs) can be leveraged to achieve user-driven clustering, emphasizing their adaptability to user-specified semantic requirements. However, directly using MLLM output for clustering has risks for producing unstructured and generic image descriptions instead of feature-specific and concrete ones. To address these issues, our method first discovers that MLLMs' hidden states of text tokens are strongly related to the corresponding features, and leverages these embeddings to perform clusterings from any user-defined criteria. We also employ a lightweight clustering head augmented with pseudo-label learning, significantly enhancing clustering accuracy. Extensive experiments demonstrate its competitive performance on diverse datasets and metrics. Codes and datasets are available in github:

Code — https://github.com/JCSTARS/Embedding-Selective-Multiple-Clustering

1 Introduction

Clustering is an unsupervised machine learning technique focused on grouping objects based on their specific patterns (Jain, Murty, and Flynn 1999; Xu and Wunsch 2005). Traditional clustering methods (MacQueen 1967; Ester et al. 1996) often rely on hand-crafted features, which can face difficulties with real-world, high-dimensional data. Deep clustering (Van Gansbeke et al. 2020; Ren et al. 2024; Caron et al. 2018) addresses this by leveraging the strong representation learning power of deep neural networks to produce feature embeddings that are more conducive to clustering. Most of these methods group the dataset with a single standard. However, users may require clustering a set of images based on multiple criteria, as illustrated in Figure 1. For instance, a set of car images can be categorized according to different attributes such as color, brand, or body style. This

scenario highlights the challenge of multi-clustering, where diverse grouping objectives coexist for the same dataset.

Multiple clustering demonstrates that a single dataset can be partitioned into distinct clusters based on different underlying structures (Yu et al. 2024). While existing methods have offered solutions for obtaining diverse clusters (Bae and Bailey 2006; Dasgupta and Ng 2010; Ren et al. 2022; Yao et al. 2023), they often rely on inherent data characteristics and lack the flexibility to directly incorporate user-defined criteria.

Foundational models like CLIP (Radford et al. 2021) recently enable clustering tasks (Yao, Qian, and Hu 2024b,a) by aligning image and text features. However, CLIP's prompt-agnostic image embeddings limit clustering based on semantic features. On the other hand, MLLMs like LLaVA (Liu et al. 2023, 2024) leverage LLMs and visual instruction tuning, enabling user-defined clustering through modality alignment.

However, naively using MLLMs for multiple clustering can face several challenges. Firstly, MLLMs tend to produce unstructured data (Li et al. 2024), making it difficult to link semantically similar outputs to specific clustering labels. Furthermore, the model's response may offer a too general image description instead of strictly following provided instructions. A comprehensive discussion of these problems is presented in Section 4.3. To mitigate these issues, we propose Embedding Selective Multiple Clustering (ESMC). As shown in Figure 2, ESMC first derives internal embeddings of text prompt tokens to extract features. These embeddings are from hidden states of text tokens of the language model in MLLMs. As visualized in Figure 3, color-related features are strongly related to the 'color' prompt token, while prompt-unrelated or image-unrelated tokens present low logits. We also employ a clustering head with pseudo-label learning to group these embeddings into well-separated clusters.

Our contributions can be summarized as follows.

- We reveal that the internal embeddings of text prompt tokens can serve as condensed representations of corresponding features and can be utilized as an effective basis for multiple clustering.
- We demonstrate that a lightweight 2-layer MLP clustering head with pseudo label supervision achieves substantial improvements.
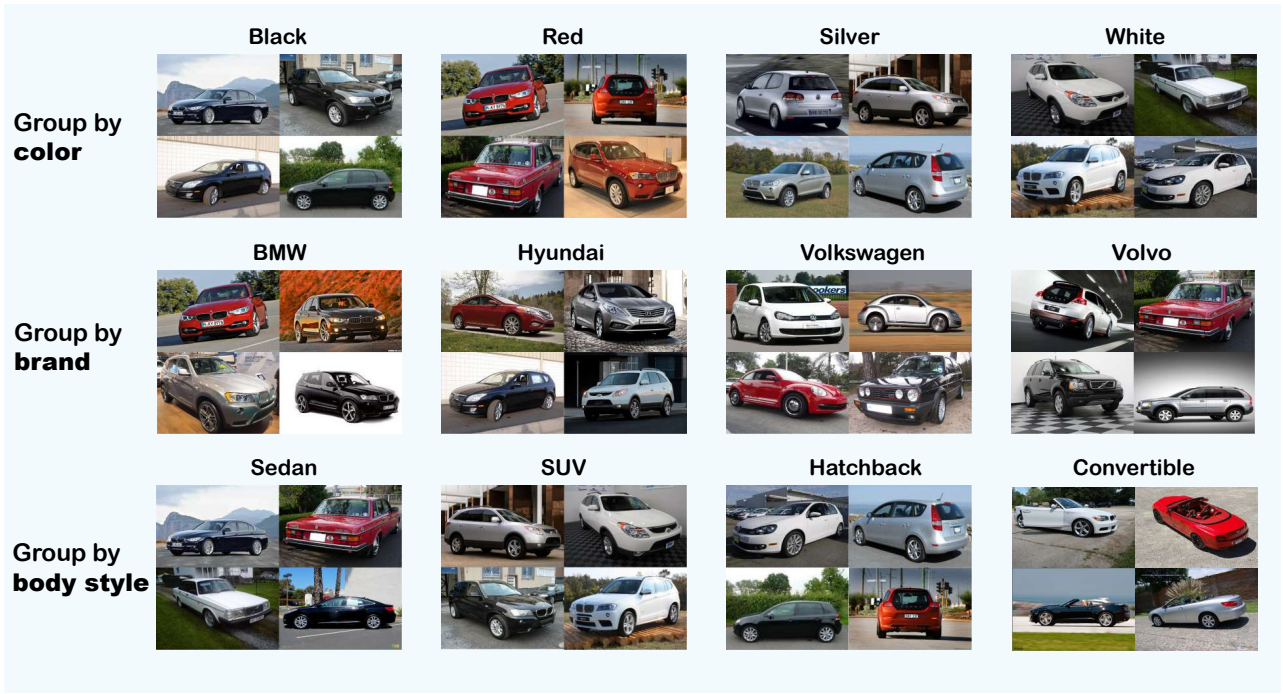
---

*Yuheng Jia is the corresponding author.

Figure 1: Multiple clustering of sample images on the Stanford_cars dataset with cluster criterion of color, manufacturer, and body style.

- Extensive experiments and ablation studies indicate that the proposed approach provides user-defined, diverse, and high-quality clustering outcomes.

2 Related Work

Multiple clustering Multiple clustering aims to discover various meaningful ways to group a dataset (Yu et al. 2024). Traditional methods often achieve this by partitioning data based on its internal characteristics, such as constructing orthogonal subspaces (Cui, Fern, and Dy 2007; Niu, Dy, and Jordan 2013) or modeling independent mixture distributions (Jain, Meka, and Dhillon 2008; Tokuda et al. 2017), employing objective functions to improve both cluster quality and diversity (Yu et al. 2024). Recent deep learning advancements have also offered improved solutions using techniques like autoencoders, muMeasuring statistical dependence with Hilbert-Schmidt normsitepyao2023augdmc to learn better representations for diverse clustering. For example, MCV (Guérin and Boots 2018) utilizes different pre-trained feature extractors as diverse views for the same data to construct multiple clusters. ENRC (Miklautz et al. 2020) finds multiple non-redundant clusters in the embedded space of the autoencoder. iMClusts (Ren et al. 2022) leverages multi-head attention to generate significant subspaces and Hilbert Schmidt Independence Criterion (HSIC) (Gretton et al. 2005) to minimize their dependencies. Multi-Map and Multi-Sub utilize CLIP (Radford et al. 2021) embeddings and proxy learning to generate multiple clusters. Most previous methods cannot provide clusters based on arbitrary user-defined criteria.

Multi-modal large language models MLLMs typically integrate three core components: a vision encoder for extracting visual features, a projection network to align visual and text modalities, and an autoregressive language backbone. Taking LLaVA-1.5 (Liu et al. 2024) as an example, its architecture comprises CLIP (Radford et al. 2021) as the vision encoder, a projection module, and Vicuna-v1.5 (Zheng et al. 2023) as the language foundation. Given an input image I, the CLIP image encoder $f_{vision\_encoder}$ will provide visual vectors. A mapping network f_{proj} is applied to project image features and text features to the same space and provides X_{visual} tokens:

$$\mathbf{X}_{visual} = f_{proj}(f_{vision\_enc}(I)) \in \mathbb{R}^{n \times d_{mllm}}, \quad (1)$$

where d_{mllm} is the dimension of MLLM embedding. The input prompt S is mapped into m tokens through the tokenizer $f_{tokenizer}$ to word embeddings from f_{embed}:

$$\mathbf{X}_{text} = f_{embed}(f_{tokenizer}(S)) \in \mathbb{R}^{m \times d_{mllm}}. \quad (2)$$

The concatenated modality embeddings $[\mathbf{X}_{vis}; \mathbf{X}_{text}]$ are fed into the transformer-based language model. Let $A_l(k) \in \mathbb{R}^{d_{model}}$ denote the k-th token's representation at the l-th transformer layer, and $A_0 = [\mathbf{X}_{vis}; \mathbf{X}_{text}]$. The final output is generated from $A_L \in \mathbb{R}^{(m+n+t) \times d_{model}}$ through an unembedding matrix $\mathbf{W}u \in \mathbb{R}^{d_{model} \times |V|}$, where $|V|$ is the vocabulary size to map the embeddings to the vocabulary space, and t represents special tokens.

Cracking the Internal Mechanisms of MLLMs Detecting and understanding the internal workings of Large Language Models (LLMs) has long been recognized as crucial for trustworthy AI (Dai et al. 2022; Zou et al. 2024;
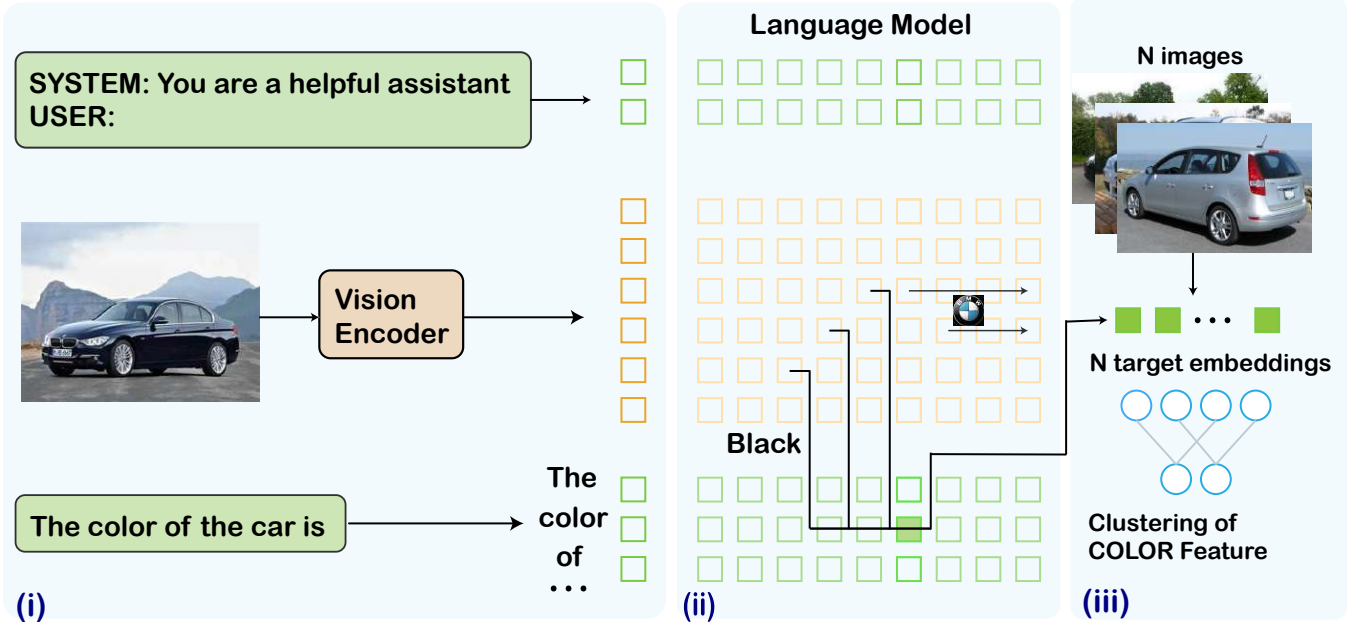
Figure 2: The ESMC framework consists of three key components: (i) the MLLM processes multimodal inputs (images and text prompts); (ii) target embeddings are selected from the language model's hidden states corresponding to text tokens; and (iii) a lightweight clustering head is trained to enhance cluster accuracy.

Zhao et al. 2024). Inspired by these works, initial efforts have explored the interpretability of Multi-modal Large Language Models (MLLMs). For instance, Vl-interp (Jiang et al. 2024) employs logit lens to identify and edit object hallucinations. LLaVA-interp (Neo et al. 2024) demonstrates a strong spatial correlation between object information and its original image location, indicating a refinement of visual input into interpretable language tokens. LVLM-interp (Ben Melech Stan et al. 2024) introduces interactive tools such as attention maps and causal graphs to aid in LVLM interpretation. However, these investigations have primarily focused on the visual processing aspects of LVLMs, leaving the internal mechanisms related to prompt token embeddings unexplored, which motivates our work.

The logit lens (nostalgebraist 2020; Belrose et al. 2023; Pal et al. 2023) serves as an interpretability technique for analyzing language models by projecting intermediate layer representations through the unembedding matrix $\mathbf{W}_u$. Specifically, it computes linguistic probabilities via:

$$E_l(k) = \mathbf{W}_u \cdot A_l(k) \in \mathbb{R}^{|V|}, \tag{3}$$

where $E_l(k)$ denotes the k-th embedding feature of l-th layer in vocabulary space. While logit lens has been utilized as a tool to understand LLMs' hidden states, our proposed method first extends its application to explain prompt tokens and their semantic relationships with visual features in MLLMs.

3 Multiple Clustering with MLLM Hidden Embedding and Lightweight Clustering Head

We leverage user-defined prompts to specify clustering criteria and present our proposed pipeline as a two-stage framework:

Target embedding extraction Based on our novel observation of feature-related embeddings from text token embeddings, we sample a few images to get precise target embeddings, as described in detail in Section 3.1.

Clustering head training A lightweight clustering head is trained to enhance clustering performance. This network transforms raw embeddings into a structured latent space suitable for clustering, which is elaborated in Section 3.2.

3.1 Find Target Embeddings

We observe that specific prompt token shows strong correlations with semantically related visual features. The positions of these embeddings are determined by the input prompt tokens. For example, as shown in Figure 3, the ground-truth labels for color and brand features are "black" and "Volvo", respectively. The color-related feature of the input image (e.g., "black") correlates strongly with the embeddings at position $E_l(263)$, which corresponds to the "color" prompt token. Similarly, the brand-related feature (e.g., "Volvo") also shows high logits in the embeddings at position $E_l(263)$, aligning with the "brand" prompt token. Conversely, features not present in the image, such as "red" for color or "BMW" for brand, exhibit significantly lower logits in their respective embeddings, enabling clear distinctions between

different features. Additional examples are provided in Appendix A.2. Further analysis on the robustness of the prompt chosen can be found in Appendix A.5.

Though selecting embeddings from later layers corresponding to specific input tokens provides reasonable performance, we propose a refined approach to enhance clustering accuracy and semantic feature representation. Specifically, we recommend sampling a small set of images, like 10 examples for each feature, to identify embeddings with high contextual specificity, followed by 2 steps:

Keyword generation We use GPT-4 to generate feature-relevant keywords (e.g., asking "What are common car colors?" and GPT would provide tokens like "white", "black", "blue", "red", etc, as a response). These keywords are crucial to locate the embedding positions.

Embedding localization For each keyword, we track the embeddings of the sampled images with top-k logit and choose the final target embeddings from those with top-k logit shared by different keywords. For example, we choose the "black" keyword generated by GPT-4, and black cars are included in the sample of images, as indicated in Figure 3. The "black" token should present high logits in embeddings like $E_{27}(263)$, $E_{28}(263)$, $E_{29}(263)$ and $E_{30}(263)$. These embeddings are candidates for target embeddings. We define logit values exceeding 0.2 as high logits (Jiang et al. 2024). More details regarding the impact of sampled image quantity and Keyword generation on performance can be found in Appendix A.6.

3.2 Pseudo Label Clustering Head training

While typical clustering methods like K-means (MacQueen 1967) can be applied directly to target embeddings from user-defined prompt criteria, we observe that raw hidden state embeddings from LLMs/MLLMs often exhibit suboptimal performance in clustering tasks (Petukhova, Matos-Carvalho, and Fachada 2025). To mitigate this limitation, our approach incorporates a two-layer MLP clustering head to align high-dimensional embeddings with low-level semantic clusters.

The procedure is formalized as follows:

Initialization Clusters are initialized via K-means. Given $\mathcal{X} = x_1, x_2, \ldots, x_N$ where $x_i \in \mathbb{R}^{|V|}$, we initialize clusters using K-means:

$$C_1, C_2, \ldots, C_K = \arg\min_{C_k} \sum_{k=1}^{K} \sum_{x_i \in C_k} \|x_i - \mu_k\|^2, \quad (4)$$

where K is the given number of target clusters. N is the number of clustering samples. $\mu_k \in \mathbb{R}^d$ is the centroid of cluster C_k. x_i is the target embedding of $E_l(k)$

Pseudo-label generation For each cluster C_j with centroid μ_j, calculate the squared Euclidean distance between each data point $x_i \in C_j$ and its cluster centroid:

$$d_{ij} = ||x_i - \mu_j||^2. \quad (5)$$

For each cluster C_j, select the top α percent of data points that have the smallest distances d_{ij} to the cluster centroid μ_j.

Let S_j be the set of these selected data points from cluster C_j, where α is a hyperparameter. Assign the pseudo-label $y_i = j$ to each selected data point $x_i \in S_j$. This creates a pseudo-labeled training set:

$$D_{pseudo} = (x_i, y_i) \mid x_i \in \bigcup_{j=1}^{k} Sj. \quad (6)$$

Network training The MLP is trained using these pseudo-labeled samples with cross-entropy loss to optimize clustering accuracy. The loss function can be denoted as:

$$L = -\frac{1}{k} \sum_{i=1}^{k} \sum_{j=1}^{C} y_{ij} \log(\hat{y}_{ij}). \quad (7)$$

4 Experiments

4.1 Experiment Setup

Datasets We evaluate our method on seven multi-clustering benchmark datasets: Stanford_Cars (Yao, Qian, and Hu 2024a) includes two criteria: *color* (red, black, white, silver) and *type* (BMW, Hyundai, Volkswagen, Volvo). Flower dataset (Yao, Qian, and Hu 2024a) contains: *species* (daisy, hyacinth, lily, rose) and *color* (pink, purple, red, white, yellow). Fruit (Hu et al. 2017) also contains two clustering criteria, *color* (red, green, yellow) and *species* (apple, banana, grape). Card (Yao et al. 2023) includes two criteria, *number* (ace to king) and *suits* (spades, clubs, hearts, diamonds). CMU_face (Günnemann et al. 2014) comprises three criteria, *emotion* (happy, sad, neutral, angry), *pose* (left, right, up, straight), and *glasses presence* (wearing sunglasses or not). Fruit360 (Yao et al. 2023) extends the Fruit dataset with additional samples: *color* (red, green, yellow, burgundy) and *species* (apple, banana, grape, cherry). CIFAR10 (Yao, Qian, and Hu 2024b)features two criteria, *environment* (sea, sky, land) and *object type* (animals, transportation). For the Flower and Stanford_Cars datasets, we extend prior work (Yao, Qian, and Hu 2024b) by constructing multi-criteria benchmarks based on dataset descriptions. The datasets are openly released with our codes.

Implementation details Target embeddings are extracted from the hidden states of LLaVA-1.5-7b (Liu et al. 2024) during inference, while user-defined criteria are encoded via prompts such as "The manufacturer of the car is", "The species of the fruit is", and "The color of the flower is." The pseudo-label ratio hyperparameter α is empirically set to 0.1 for the CMU_face and Card dataset, 0.2 for Fruit360 and CIFAR10 datasets, 0.3 for Stanford_cars and Flower datasets, and 0.4 for Fruit datasets. The clustering head is implemented as a two-layer MLP, with the first layer mapping the input dimension $|V|$ to 512 units and the second layer projecting these features to the target cluster number. We train the clustering head for 100 epochs. We employ Normalized Mutual Information (NMI) (Meilă 2007) and the Rand Index (RI) (Rand 1971) as external metrics to measure the similarity between clustering results and ground truth. The experiments are conducted on one RTX3090 card with 24GB of memory.
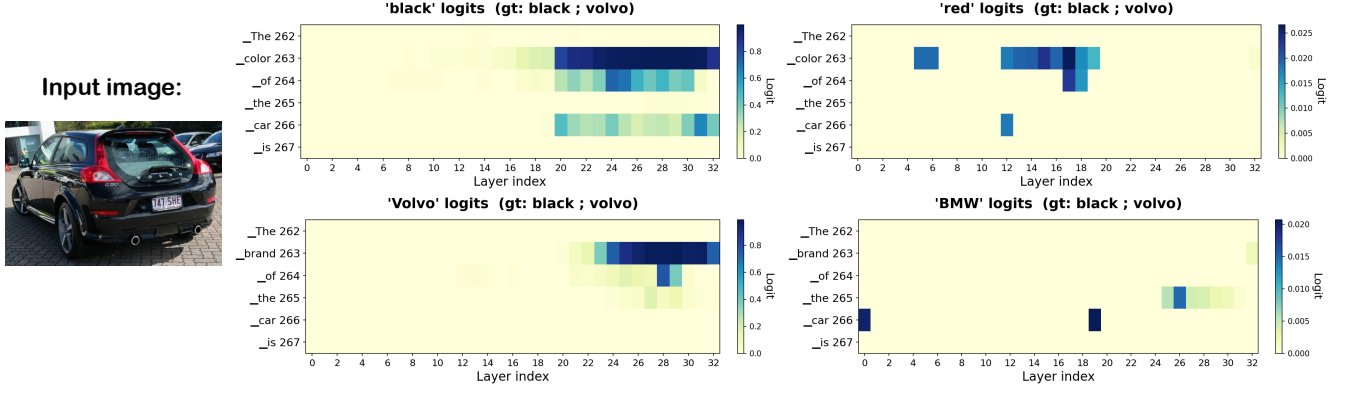
Figure 3: The relationship between vocabulary logits and text prompt tokens, note that the color bar varies across the figures. The image is from the Stanford_cars dataset.

4.2 Results

As presented in Tables 1 and 2, the proposed ESMC method demonstrates overall superior performance compared to baselines across various clustering tasks and datasets, evidenced by its NMI and RI scores. On CIFAR10-Type, ESMC achieved the top NMI (0.8293) and RI (0.9520), marking a significant improvement over Multi-Sub (0.5271 for NMI, 0.7394 for RI) and Multi-Map (0.4967 for NMI, 0.7104 for RI). ESMC also exceeded baseline results for Fruit-Species, CMU_face-Glass, Flower dataset, CIFAR-10 dataset, and Stanford_Cars-Type datasets. It obtained perfect scores for Fruit-Species and achieved leading scores of NMI 0.8923 and RI 0.9726 on Flower-Species, surpassing Multi-Sub's NMI by 21.09%.

We note minor underperformance in the Fruit360-Color NMI and Fruit NMI scores. This may arise from the characteristics of the datasets, such as unclear images, and differences in the internal knowledge of the underlying models (e.g., LLaVA and CLIP). For instance, our analysis, detailed in Appendix A.4, reveals instances where models misidentified colors or object types due to ambiguous visual cues. Previous methods like Multi-Map and Multi-Sub, often relying on specific keywords, exhibit fewer such ambiguities.

4.3 Ablation Studies

Clustering of MLLM outputs yields suboptimal performance To evaluate the limitations of clustering directly by the MLLM linguistic output, we compare our method with a baseline approach that clusters text outputs from LLaVA. Specifically, we first extract textual outputs from the model and generate semantic embeddings by feeding them into the CLIP text encoder (Radford et al. 2021). Experimental results (Table 3) confirm that our proposed approach outperforms this clustering strategy. The inferior performance of the baseline arises from three key factors. Firstly, the unstructured nature of MLLM outputs introduces inconsistent responses to inputs. As shown in Figure 4, when presented with two images of the same environment type described as "The background environment is a cloudy sky" and a much longer description, the CLIP text encoder may fail to pro-
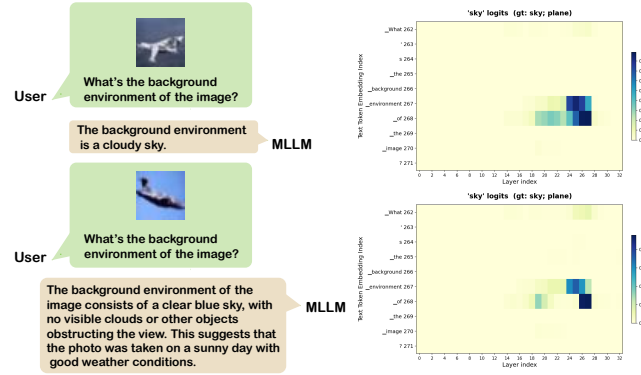

Figure 4: Left: Two MLLM outputs with shared semantic meaning but distinct formatting. Right: The target embedding we choose $E_{25}(267)$, shows higher consistency in "sky" logit, as the clustering label in the environment criterion.

duce semantically aligned embeddings. In contrast, MLLM embeddings from ESMC assign nearly identical logits to the "sky" token (0.8194 and 0.7436), which suggests consistency in semantic representation, particularly after applying the softmax function to embedding logits. These two images are highly likely to be clustered together due to their shared environmental features.

Secondly, MLLM tends to provide overly general descriptions instead of specific features. As illustrated in Figure 5, when prompted with "The species of the flower is", the model responds "pink rose" instead of focusing on the species feature. This conflates distinct attributes like color and species, making it harder to cluster based on precise criteria.

Thirdly, language bias (He et al. 2025; Leng et al. 2024; Lee et al. 2024)—MLLM's tendency to prioritize prior linguistic knowledge over visual context—directly contributes to performance gaps. This bias creates a critical trade-off: excessive reliance on language priors may induce hallucinations, which happen when MLLMs generate outputs incon-

Dataset	Criteria	MCV	ENRC	iMClusts	AugDMC	DDMC	Multi-Map	Multi-Sub	**ESMC**
Stanford_Cars	Color	0.2103	0.2465	0.2336	0.2736	0.6899	0.7360	<u>0.7533</u>	**0.8138**
	Type	0.1650	0.2063	0.1963	0.2364	0.6045	0.6355	<u>0.6616</u>	**0.8817**
Flowers	Color	0.2938	0.3329	0.3169	0.3556	0.6327	0.6426	<u>0.6940</u>	**0.7283**
	Species	0.1326	0.1561	0.1894	0.1887	0.1996	0.6148	<u>0.7580</u>	**0.8923**
CIFAR-10	Type	0.1618	0.1826	0.2040	0.2855	0.3991	0.4967	<u>0.5271</u>	**0.8293**
	Environment	0.1379	0.1892	0.1920	0.2927	0.3782	0.4598	<u>0.4828</u>	**0.6075**
CMU_face	Emotion	0.1433	0.1592	0.0422	0.0161	0.1726	0.1786	<u>0.2053</u>	**0.2237**
	Glass	0.1201	0.1493	0.1299	0.1039	0.2261	0.3402	<u>0.4870</u>	**0.7665**
	Pose	0.3254	0.2290	0.4437	0.1320	0.4526	0.4693	<u>0.5923</u>	**0.6271**
Card	Order	0.0792	0.1225	0.1144	0.1440	0.1563	0.3633	<u>0.3921</u>	**0.4736**
	Suits	0.0430	0.0676	0.0716	0.0873	0.0933	0.2734	<u>0.3104</u>	**0.3586**
Fruit360	Color	0.3777	0.4264	0.4097	0.4594	0.4981	0.6239	0.6654	**0.6952**
	Species	0.2985	0.4142	0.3861	0.5139	<u>0.5292</u>	0.5284	**0.6123**	0.5036
Fruit	Color	0.6266	0.7103	0.7351	0.8517	0.8973	0.8619	**0.9693**	<u>0.9308</u>
	Species	0.2733	0.3187	0.3029	0.3546	0.3764	1.0000	<u>1.0000</u>	**1.0000**

Table 1: Quantitative comparison of 8 approaches using NMI. For methods involving k-means, the average result of 10 times is reported.

Dataset	Criteria	MCV	ENRC	iMClusts	AugDMC	DDMC	Multi-Map	Multi-Sub	**ESMC**
Stanford_Cars	Color	0.5802	0.6779	0.6552	0.7525	0.8765	0.9193	**0.9387**	<u>0.9235</u>
	Type	0.5634	0.6217	0.5643	0.7356	0.7957	0.8399	<u>0.8792</u>	**0.9589**
Flowers	Color	0.5860	0.6214	0.6127	0.6931	0.7887	0.7984	<u>0.8843</u>	**0.8992**
	Species	0.5273	0.6065	0.6195	0.6077	0.6227	0.8321	<u>0.8980</u>	**0.9726**
CIFAR-10	Type	0.5634	0.6217	0.5643	0.7356	0.7957	0.8399	<u>0.7394</u>	**0.9589**
	Environment	0.3344	0.3599	0.3664	0.4689	0.5547	0.6737	<u>0.7096</u>	**0.8282**
CMU_face	Emotion	0.5268	0.6630	0.5932	0.5367	0.7593	<u>0.7105</u>	**0.8527**	0.6697
	Glass	0.4955	0.6209	0.5627	0.5361	0.7663	0.7068	<u>0.8324</u>	**0.9259**
	Pose	0.6028	0.5029	0.6114	0.5517	0.7904	0.6624	**0.8736**	<u>0.8253</u>
Card	Order	0.7128	0.7313	0.7658	0.8267	0.8326	0.8587	**0.8842**	<u>0.8805</u>
	Suits	0.3638	0.3801	0.3715	0.4228	0.6469	0.7039	**0.8504**	<u>0.7285</u>
Fruit360	Color	0.6791	0.6868	0.6841	0.7392	0.7472	0.8439	**0.8821**	<u>0.8493</u>
	Species	0.6176	0.6984	0.6732	0.7430	<u>0.7703</u>	0.7582	**0.8504**	0.7285
Fruit	Color	0.7685	0.8511	0.8632	0.9108	0.9383	0.9556	**0.9964**	<u>0.9732</u>
	Species	0.6597	0.6536	0.6743	0.7399	0.7621	1.0000	<u>1.0000</u>	**1.0000**

Table 2: Quantitative comparison of 8 approaches using RI. For methods involving k-means, the average result of 10 times is reported.

sistent with images, while underweighting linguistic guidance risks losing discriminative information encoded in the input prompts.

The proposed approach, ESMC, leverages intermediate hidden states from earlier layers of the MLLM, rather than the final output layer. This design not only preserves the text prompt's semantic guidance through embeddings at special positions encoded by quantized probability but also mitigates language bias by avoiding the dominance of higher-level of linguistic abstractions in later auto-regressive layers, which are prone to over-reliance on previously generated responses. By doing so, we ensure that our target embeddings are grounded in the initial, raw fusion of visual and linguistic information, while with less linguistic bias or language priors(Lin et al. 2024) from the luanguage model itself.

Clustering head improves performance Clustering head (Van Gansbeke et al. 2020; Niu, Shan, and Wang 2022; Jia et al. 2025) is a lightweight and effective technique for enhancing clustering performance. Our results, presented as NMI and RI gains in Table 3, show that the inclusion of a

Dataset	Criteria	NMI↑			RI↑		
		Output	ESMC, w/o.MLP	**ESMC**	Output	ESMC, w/o.MLP	**ESMC**
Stanford_Cars	Color	0.7871	0.7934	**0.8138**	0.9107	0.9129	**0.9235**
	Type	0.6462	0.8694	**0.8817**	0.8474	0.9517	**0.9589**
Flower	Color	0.6698	0.6835	**0.7283**	0.8736	0.8810	**0.8982**
	Species	0.8133	0.8462	**0.8923**	0.9329	0.9347	**0.9726**
CIFAR-10	Type	0.7505	0.7149	**0.8293**	0.8953	0.9137	**0.9520**
	Environment	0.0443	0.5484	**0.6075**	0.4941	0.7860	**0.8282**
CMU_face	Emotion	0.1498	0.1902	**0.2237**	0.5876	0.6346	**0.6697**
	Glass	0.6780	0.6445	**0.7665**	0.8279	0.7955	**0.9259**
	Pose	0.0913	0.5498	**0.6271**	0.5631	0.8140	**0.8253**
Card	Order	0.4387	0.3895	**0.4736**	0.8348	0.8712	**0.8805**
	Suits	0.2423	0.3334	**0.3586**	0.4258	0.6982	**0.7258**
Fruit360	Color	0.6071	0.6523	**0.6952**	0.7972	0.7584	**0.8493**
	Species	0.2199	0.3806	**0.5036**	0.5080	0.6824	**0.7285**
Fruit	Color	0.9308	0.9308	0.9308	0.9732	0.9732	0.9732
	Species	0.8441	1.0000	**1.0000**	0.9337	1.0000	**1.0000**

Table 3: The table compares three clustering approaches: (1) Output (direct clustering using the model's linguistic output), (2) Ours, w/o.MLP (clustering without an MLP-based clustering head), and (3) ESMC (The proposed approach). We do not present the results of adding the clustering head after the MLLM output with CLIP embeddings due to significant performance degradation.

Dataset	Stanford_cars	Flower	CIFAR-10	CMU_face	Card	Fruit360	Fruit
time/s	0.3675	0.4472	15.03	0.5016	4.636	2.874	0.3968

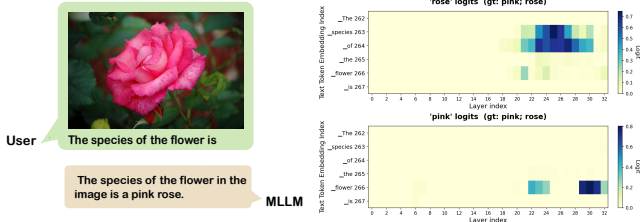Table 4: Total training time (100 epochs with different features) for clustering heads.

Figure 5: Left: Conversation reveals that the MLLM response can be too general. It responds as "pink rose" instead of "rose" directly, while we only care about the species feature instead of the color feature. Right: Our target embedding $E_{25}(263)$ shows high logit in "rose" logit and low in "pink" logit, which could indicate the species feature.

clustering head can lead to substantial improvements, reaching up to 12% on the Fruit360 dataset of species feature and the CMU_face dataset of Glass feature. This benefit is likely due to the high dimensionality of the MLLM embeddings after projection into the vocabulary space, causing the curse of dimensionality(Indyk and Motwani 1998; Donoho et al. 2000). Although ESMC embeddings provide richer feature representations, they seem less directly suited for clustering.

Notably, we observed that the clustering head did not enhance performance when applying CLIP embeddings, likely because these embeddings already exhibit a strong inherent capacity for clustering in semantic spaces. The clustering head is also highly time-efficient, with the only trainable part is the 2-layer MLP head, resulting in significantly smaller FLOPs and memory usage compared to previous method(Yao, Qian, and Hu 2024b), which is detailed in Table 4.

5 Conclusion and Limitation

In conclusion, our proposed method, ESMC, introduces an explainable framework for multiple clustering tasks, addressing limitations of existing multimodal language models (MLLMs). While MLLMs excel in visual feature extraction and contextual knowledge, they can yield unstructured or overly generic interpretations. To mitigate this, ESMC obtains target embeddings via sampling and employs a lightweight clustering head with pseudo-label learning for well-separated clusters. The method's transparency is grounded in the use of specific, interpretable text token embeddings as the clustering basis. By focusing the clustering process on these features, ESMC not only leverages the strengths of MLLMs but also enhances the interpretability of their internal representations. We also present the limitations

and future directions.

Specific language model architecture Based on our study, MLLMs like LLaVA, built on LLaMA (Touvron et al. 2023), exhibit specific text prompt embedding properties. We found this architecture type fuses text and image features at a relatively late stage, with vision features injected as visual tokens.

Future work While our work focused on applying text prompt embeddings to multiple clustering tasks, we believe MLLMs offer other effective ways for clustering or retrieval. Our research may also aid MLLM interpretability and grounding techniques. Ultimately, we aim for this work to foster more reliable and safer MLLM.

References

Bae, E.; and Bailey, J. 2006. Coala: A novel approach for the extraction of an alternate clustering of high quality and high dissimilarity. In *Sixth International Conference on Data Mining*, 53–62. IEEE.

Belrose, N.; Furman, Z.; Smith, L.; Halawi, D.; Ostrovsky, I.; McKinney, L.; Biderman, S.; and Steinhardt, J. 2023. Eliciting latent predictions from transformers with the tuned lens. *arXiv preprint arXiv:2303.08112*.

Ben Melech Stan, G.; Aflalo, E.; Rohekar, R. Y.; Bhiwandiwalla, A.; Tseng, S.-Y.; Olson, M. L.; Gurwicz, Y.; Wu, C.; Duan, N.; and Lal, V. 2024. Lvlm-intrepret: An interpretability tool for large vision-language models. In *Proceedings of the IEEE/CVF Conference on Computer Vision and Pattern Recognition*, 8182–8187.

Caron, M.; Bojanowski, P.; Joulin, A.; and Douze, M. 2018. Deep clustering for unsupervised learning of visual features. In *Proceedings of the European conference on computer vision*, 132–149.

Comanici, G.; Bieber, E.; Schaekermann, M.; Pasupat, I.; Sachdeva, N.; Dhillon, I.; Blistein, M.; Ram, O.; Zhang, D.; Rosen, E.; et al. 2025. Gemini 2.5: Pushing the frontier with advanced reasoning, multimodality, long context, and next generation agentic capabilities. *arXiv preprint arXiv:2507.06261*.

Cui, Y.; Fern, X. Z.; and Dy, J. G. 2007. Non-redundant multi-view clustering via orthogonalization. In *Seventh IEEE international conference on data mining*, 133–142. IEEE.

Dai, D.; Dong, L.; Hao, Y.; Sui, Z.; Chang, B.; and Wei, F. 2022. Knowledge neurons in pretrained transformers. In *Proceedings of the 60th Annual Meeting of the Association for Computational Linguistics (Volume 1: Long Papers)*, 8493–8502.

Dasgupta, S.; and Ng, V. 2010. Mining clustering dimensions. In *Proceedings of the 27th International Conference on Machine Learning*, 263–270.

Donoho, D. L.; et al. 2000. High-dimensional data analysis: The curses and blessings of dimensionality. *AMS math challenges lecture*, 1(2000): 32.

Ester, M.; Kriegel, H.-P.; Sander, J.; and Xu, X. 1996. A density-based algorithm for discovering clusters in large spatial databases with noise. In *Proceedings of the Second International Conference on Knowledge Discovery and Data Mining*, 226–231.

Gretton, A.; Bousquet, O.; Smola, A.; and Schölkopf, B. 2005. Measuring statistical dependence with Hilbert-Schmidt norms. In *International conference on algorithmic learning theory*, 63–77. Springer.

Guérin, J.; and Boots, B. 2018. Improving image clustering with multiple pretrained cnn feature extractors. *arXiv preprint arXiv:1807.07760*.

Günnemann, S.; Färber, I.; Rüdiger, M.; and Seidl, T. 2014. Smvc: semi-supervised multi-view clustering in subspace projections. In *Proceedings of the 20th ACM SIGKDD international conference on Knowledge discovery and data mining*, 253–262.

Guo, D.; Yang, D.; Zhang, H.; Song, J.; Zhang, R.; Xu, R.; Zhu, Q.; Ma, S.; Wang, P.; Bi, X.; et al. 2025. Deepseek-r1: Incentivizing reasoning capability in llms via reinforcement learning. *arXiv preprint arXiv:2501.12948*.

He, J.; Zhu, K.; Guo, H.; Fang, J.; Hua, Z.; Jia, Y.; Tang, M.; Chua, T.-S.; and Wang, J. 2025. Cracking the code of hallucination in lvlms with vision-aware head divergence. In *Proceedings of the 63rd Annual Meeting of the Association for Computational Linguistics (Volume 1: Long Papers)*, 3488–3501.

Hu, J.; Qian, Q.; Pei, J.; Jin, R.; and Zhu, S. 2017. Finding multiple stable clusterings. *Knowledge and Information Systems*, 51: 991–1021.

Indyk, P.; and Motwani, R. 1998. Approximate nearest neighbors: towards removing the curse of dimensionality. In *Proceedings of the thirtieth annual ACM symposium on Theory of computing*, 604–613.

Jain, A. K.; Murty, M. N.; and Flynn, P. J. 1999. Data clustering: a review. *ACM computing surveys*, 31(3): 264–323.

Jain, P.; Meka, R.; and Dhillon, I. S. 2008. Simultaneous Unsupervised Learning of Disparate Clusterings. *Statistical Analysis and Data Mining*, 1(3): 195–210.

Jia, Y.; Cheng, J.; Liu, H.; and Hou, J. 2025. Towards Calibrated Deep Clustering Network. In *The Thirteenth International Conference on Learning Representations*.

Jiang, N.; Kachinthaya, A.; Petryk, S.; and Gandelsman, Y. 2024. Interpreting and editing vision-language representations to mitigate hallucinations. *arXiv preprint arXiv:2410.02762*.

Lee, S.; Park, S. H.; Jo, Y.; and Seo, M. 2024. Volcano: mitigating multimodal hallucination through self-feedback guided revision. In *Proceedings of the 2024 Conference of the North American Chapter of the Association for Computational Linguistics: Human Language Technologies (Volume 1: Long Papers)*, 391–404.

Leng, S.; Zhang, H.; Chen, G.; Li, X.; Lu, S.; Miao, C.; and Bing, L. 2024. Mitigating object hallucinations in large vision-language models through visual contrastive decoding. In *Proceedings of the IEEE/CVF Conference on Computer Vision and Pattern Recognition*, 13872–13882.

Li, D.; Zhao, Y.; Wang, Z.; Jung, C.; and Zhang, Z. 2024. Large Language Model-Driven Structured Output: A Comprehensive Benchmark and Spatial Data Generation Framework. *ISPRS International Journal of Geo-Information*, 13(11): 405.

Lin, Z.; Chen, X.; Pathak, D.; Zhang, P.; and Ramanan, D. 2024. Revisiting the role of language priors in vision-language models. In *Proceedings of the 41st International Conference on Machine Learning*, volume 1205.

Liu, H.; Li, C.; Li, Y.; and Lee, Y. J. 2024. Improved baselines with visual instruction tuning. In *Proceedings of the IEEE/CVF Conference on Computer Vision and Pattern Recognition*, 26296–26306.

Liu, H.; Li, C.; Wu, Q.; and Lee, Y. J. 2023. Visual instruction tuning. *Advances in neural information processing systems*, 36: 34892–34916.

MacQueen, J. 1967. Some methods for classification and analysis of multivariate observations. In *Proceedings of the Fifth Berkeley Symposium on Mathematical Statistics and Probability, Volume 1: Statistics*, volume 5, 281–298. University of California press.

Meilă, M. 2007. Comparing clusterings—an information based distance. *Journal of multivariate analysis*, 98(5): 873–895.

Miklautz, L.; Mautz, D.; Altinigneli, M. C.; Böhm, C.; and Plant, C. 2020. Deep embedded non-redundant clustering. In *Proceedings of the AAAI conference on artificial intelligence*, volume 34, 5174–5181.

Neo, C.; Ong, L.; Torr, P.; Geva, M.; Krueger, D.; and Barez, F. 2024. Towards interpreting visual information processing in vision-language models. *arXiv preprint arXiv:2410.07149*.

Niu, C.; Shan, H.; and Wang, G. 2022. Spice: Semantic pseudo-labeling for image clustering. *IEEE Transactions on Image Processing*, 31: 7264–7278.

Niu, D.; Dy, J. G.; and Jordan, M. I. 2013. Iterative discovery of multiple alternativeclustering views. *IEEE transactions on pattern analysis and machine intelligence*, 36(7): 1340–1353.

nostalgebraist. 2020. Interpreting GPT: The Logit Lens. https://www.lesswrong.com/posts/AcKRB8wDpdaN6v6ru/interpreting-gpt-the-logit-lens.

Pal, K.; Sun, J.; Yuan, A.; Wallace, B. C.; and Bau, D. 2023. Future Lens: Anticipating Subsequent Tokens from a Single Hidden State. In *Proceedings of the 27th Conference on Computational Natural Language Learning*, 548–560.

Petukhova, A.; Matos-Carvalho, J. P.; and Fachada, N. 2025. Text clustering with large language model embeddings. *International Journal of Cognitive Computing in Engineering*, 6: 100–108.

Radford, A.; Kim, J. W.; Hallacy, C.; Ramesh, A.; Goh, G.; Agarwal, S.; Sastry, G.; Askell, A.; Mishkin, P.; Clark, J.; et al. 2021. Learning transferable visual models from natural language supervision. In *International conference on machine learning*, 8748–8763. PmLR.

Rand, W. M. 1971. Objective criteria for the evaluation of clustering methods. *Journal of the American Statistical association*, 66(336): 846–850.

Ren, L.; Yu, G.; Wang, J.; Liu, L.; Domeniconi, C.; and Zhang, X. 2022. A diversified attention model for interpretable multiple clusterings. *IEEE Transactions on Knowledge and Data Engineering*, 35(9): 8852–8864.

Ren, Y.; Pu, J.; Yang, Z.; Xu, J.; Li, G.; Pu, X.; Yu, P. S.; and He, L. 2024. Deep clustering: A comprehensive survey. *IEEE transactions on neural networks and learning systems*.

Tokuda, T.; Yoshimoto, J.; Shimizu, Y.; Okada, G.; Takamura, M.; Okamoto, Y.; Yamawaki, S.; and Doya, K. 2017. Multiple co-clustering based on nonparametric mixture models with heterogeneous marginal distributions. *PloS one*, 12(10): e0186566.

Van Gansbeke, W.; Vandenhende, S.; Georgoulis, S.; Proesmans, M.; and Van Gool, L. 2020. Scan: Learning to classify images without labels. In *European conference on computer vision*, 268–285. Springer.

Xu, R.; and Wunsch, D. 2005. Survey of clustering algorithms. *IEEE Transactions on neural networks*, 16(3): 645–678.

Yao, J.; Liu, E.; Rashid, M.; and Hu, J. 2023. Augdmc: Data augmentation guided deep multiple clustering. *Procedia Computer Science*, 222: 571–580.

Yao, J.; Qian, Q.; and Hu, J. 2024a. Customized multiple clustering via multi-modal subspace proxy learning. In *Proceedings of the 38th International Conference on Neural Information Processing Systems*, 82705–82725.

Yao, J.; Qian, Q.; and Hu, J. 2024b. Multi-modal proxy learning towards personalized visual multiple clustering. In *Proceedings of the IEEE/CVF Conference on Computer Vision and Pattern Recognition*, 14066–14075.

Yu, G.; Ren, L.; Wang, J.; Domeniconi, C.; and Zhang, X. 2024. Multiple clusterings: Recent advances and perspectives. *Computer Science Review*, 52: 100621.

Zhao, H.; Chen, H.; Yang, F.; Liu, N.; Deng, H.; Cai, H.; Wang, S.; Yin, D.; and Du, M. 2024. Explainability for large language models: A survey. *ACM Transactions on Intelligent Systems and Technology*, 15(2): 1–38.

Zheng, L.; Chiang, W.-L.; Sheng, Y.; Zhuang, S.; Wu, Z.; Zhuang, Y.; Lin, Z.; Li, Z.; Li, D.; Xing, E.; et al. 2023. Judging llm-as-a-judge with mt-bench and chatbot arena. *Advances in Neural Information Processing Systems*, 36: 46595–46623.

Zou, A.; Phan, L.; Wang, J.; Duenas, D.; Lin, M.; Andriushchenko, M.; Kolter, J. Z.; Fredrikson, M.; and Hendrycks, D. 2024. Improving alignment and robustness with circuit breakers. *Advances in Neural Information Processing Systems*, 37: 83345–83373.

A Appendices

We include the source code for our experiments, a hyper-parameter sensitivity analysis, prompt robustness analysis, and additional examples of target embedding selection and illustrations.

A.1 Hyperparameter analysis

Here we conduct the Hyperparameter sensitivity analysis of pseudo label ratio in the Flower dataset with color and species features. As shown in Figure 6, the NMI and RI scores are generally higher than the baselines(K-means clustering without clustering heads). When α is too high or too low, the performance degrades, mainly due to introducing noisy labels and a lack of supervision, respectively.
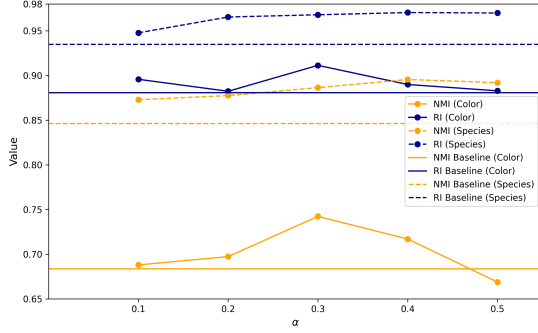

Figure 6: Hyperparameter sensitivity analysis α on Flower dataset

A.2 Target embedding examples

Here we provide more examples of target embedding selection with corresponding logits. The high logits are related to feature representative tokens like "type" and "color", as shown in Figure 7 and Figure 8. Note that when prompting the model with type features, other visual features, like color features, are not presented at the position of "type" tokens, facilitating the distinction of different features.

A.3 Algorithms

Here we present the pseudo-codes of the algorithms mentioned above.

Algorithm 1: Target Embedding Localization

1: **Input:** prompt_tokens, number of samples N, threshold τ, selection threshold θ, unembedding_matrix W
2: **Output:** Target embeddings
3: **for** each feature in prompt_tokens **do**
4:     Sample N images randomly
5:     Generate keywords using GPT-4: `keywords ←` GPT4("What are common [feature]?")
6:     **for** each keyword in keywords **do**
7:       **for** each image in sampled_images **do**
8:         hidden_states `←model.forward(image, text_prompt)·`W
9:         logit ← hidden_states[keyword]
10:         **for** each layer, position in model **do**
11:           **if** logit[layer][position] $> \tau$ **then**
12:             candidate_positions[(layer, position)] ← candidate_positions[(layer, position)] $+1$
13:           **end if**
14:         **end for**
15:       **end for**
16:     **end for**
17: **end for**
18: max_count ← $\max\{\text{count(p)} \mid \text{p} \in \text{candidate\_positions}\}$
19: target_embeddings ←$\{\text{embedding(p)} \mid \text{p} \in$ candidate_positions and count(p) = max_count$\}$
20: **return** target_embeddings

Algorithm 2: Pseudo Label Clustering head

1: **Input:** target_embeddings, number of clusters K, hyperparameter α, maximum training epochs max_epochs
2: **Output:** Predictions
3: **Initialize** clusters via K-means on target_embeddings, pseudo-labeled dataset D_{pseudo}
4: **for** each cluster C in clusters **do**
5:     Compute distances ← $\{\|x_i - \text{centroid}(C)\|^2 \mid x_i \in$ target_embeddings$\}$
6:     Sort samples by distances in ascending order
7:     D_{cluster} ←Select top $\alpha\%$ samples with smallest distances
8:     $D_{\text{pseudo}} \leftarrow D_{\text{pseudo}} \cup D_{\text{cluster}}$
9: **end for**
10: **Initialize** Clustering_head with input_dim, hidden_dim, output_dim = K
11: **for** epoch = 1 to max_epochs **do**
12:     Predictions ← Clustering_head.forward(D_{pseudo}.inputs)
13:     Loss ← CrossEntropyLoss(Predictions, D_{pseudo}.labels)
14:     Update Clustering_head parameters
15: **end for**
16: **return** Predictions

A.4 Failure Cases Analysis

We elaborate on the minor underperformance observed in the Fruit360-Species NMI and Fruit-Color NMI scores. This
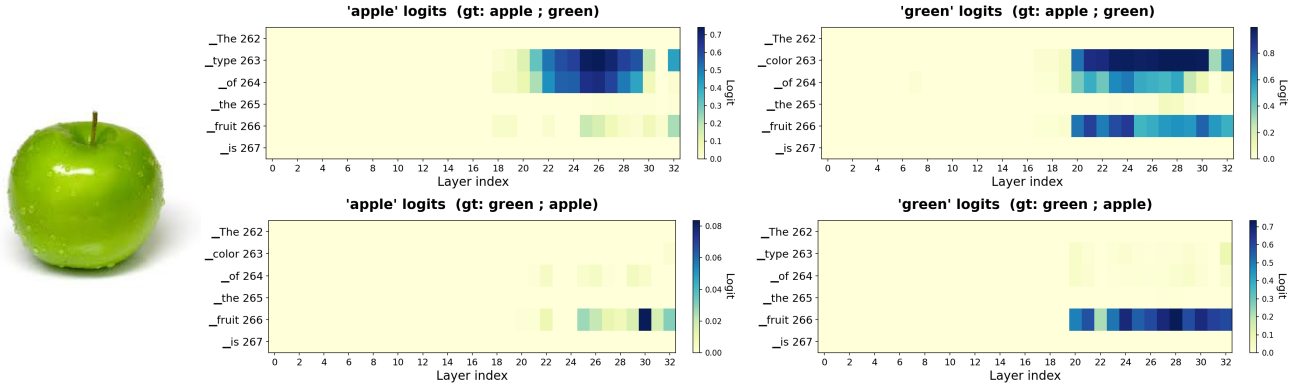
Figure 7: Color and type logits in Fruit dataset for green apple, we choose the embedding $E_{27}(263)$ for both features.
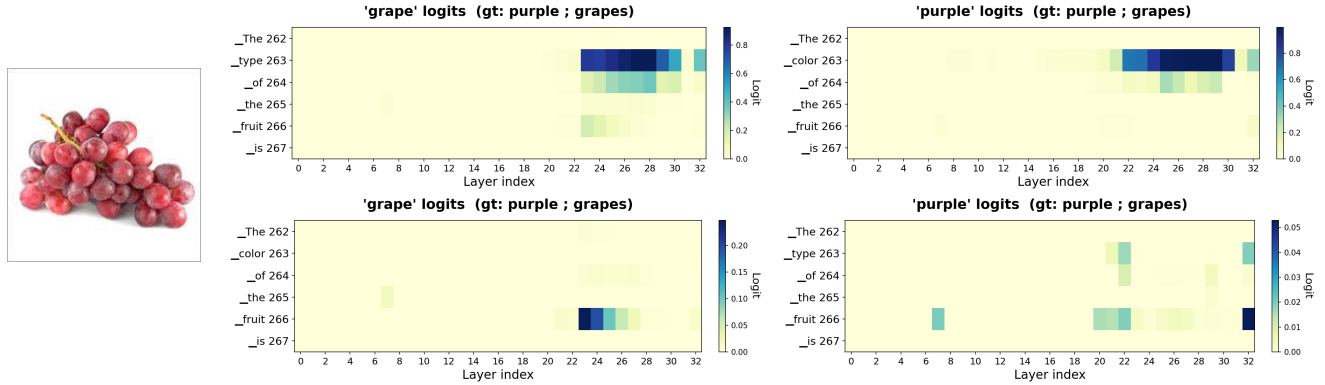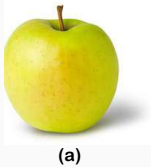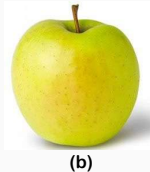

Figure 8: Color and type logits in Fruit dataset for purple grapes, we choose the embedding $E_{27}(263)$ for both features.

Figure 9: Failure cases in Fruit dataset and Fruit360 dataset

issue likely stems from the interplay of unclear image qualities within these datasets and inherent differences in the internal knowledge representations of the models used (i.e., LLaVA and CLIP). As depicted in Figure 9, for instance, a yellow apple (ground truth) is sometimes mistaken as "Green" (a,b), while other mistakes include identifying a grape as an avocado (c), a grape as a tomato (d), an apple as a potato (e), and a cherry as an orange (f). These specific errors

may occur because of the distinct internal knowledge base of LLaVA and CLIP. For example, when directly prompting the models about the color of the aforementioned yellow apple, CLIP responds that it's a yellow apple, whereas LLaVA responds that it's more likely a green apple, a perception which humans might interpret as a yellow-green apple. In contrast, previous methods such as Multi-Map and Multi-Sub exhibit fewer such misidentifications. This is primarily because they are built upon CLIP models and leverage specific keywords (e.g., grapes, apples, oranges, cherries, and bananas) explicitly provided to the model, thereby significantly reducing confusion caused by visually ambiguous images.

A.5 Prompt Robustness Analysis

The performance of methods relying on MLLMs can be sensitive to the precise phrasing of input prompts. To demonstrate the robustness of our proposed ESMC method, particularly concerning the "Embedding localization" step, this subsection analyzes its performance across various semantically equivalent but lexically diverse prompts. We designed six prompt variants for generating keywords for the "Color" and "Brand" criteria. An example set for "Color" is provided below:

- **Original:** "The color of the car is"

Prompt Variant	Criterion	NMI	RI
Original: "The color of the car is"	Color	0.8138	0.9235
Variant 1: "Color of the car:"	Color	0.8016	0.9194
Variant 2: "Identify the color of this vehicle."	Color	0.8143	0.9257
Variant 3: "Provide the exact car color."	Color	0.8113	0.9268
Original: "The brand of the car is"	Brand	0.8817	0.9589
Variant 1: "Brand of the car:"	Brand	0.8784	0.9524
Variant 2: "Tell me the make of the car."	Brand	0.8911	0.9657
Variant 3: "What's the brand of the car?"	Brand	0.8957	0.9669

Table 5: Prompt Robustness Analysis (NMI and RI on Stanford_Cars Dataset)
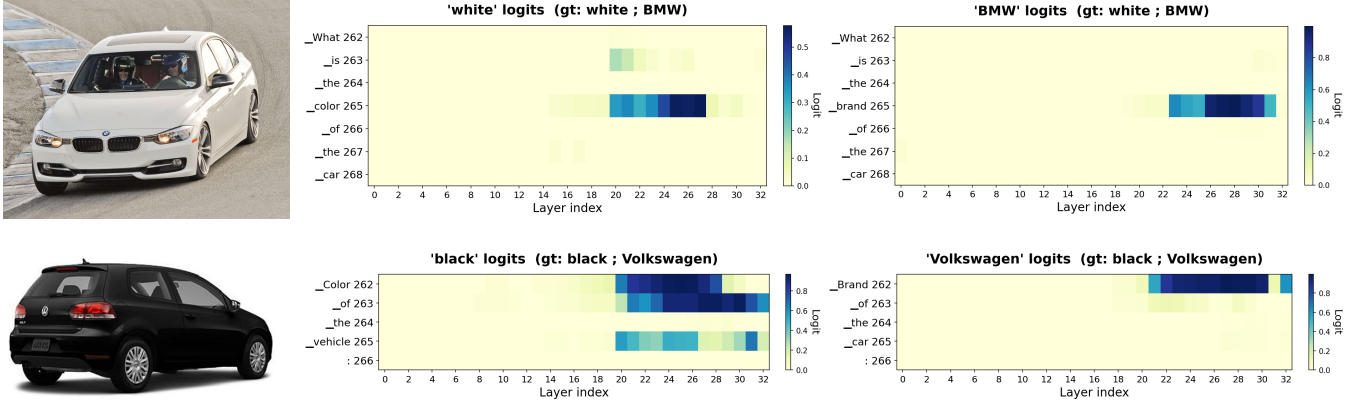

Figure 10: Token logits among different prompts for both color and brand feature.

- **Variant 1:** "Color of the car:"
- **Variant 2:** "Identify the color of this vehicle."
- **Variant 3:** "Provide the exact car color."

We applied each prompt variant to the LLaVA model with the criterion of color and brand, ran the full ESMC pipeline, and measured the NMI and RI score. We also present the visualization result in Figure 10.

As shown in Table 5, the NMI scores exhibit remarkable consistency across all tested prompt variations for the Stanford_Cars dataset. This strong performance stability confirms the robustness of our ESMC method against minor lexical changes in the prompts used for MLLM's inference. We attribute this robustness to two main factors: firstly, LLaVA's advanced semantic understanding allows it to interpret diverse phrasings with similar intent; and secondly, our "Embedding Localization" step is designed to identify stable semantic embeddings by leveraging high logits across different keywords with similar meanings.

A.6 Impact of Sampling Quantity and Keyword Selection

This section analyzes the influence of sampled image quantity and the choice of Large Language Model (LLM) for keyword generation on the accuracy of the identified target embeddings and the final clustering performance. Note that these modules would only have an impact on the target embedding chosen.

Sampled Images	Criterion	Target Embedding	NMI
3	Color	$E_{27}(263)$	0.8138
3	Brand	$E_{27}(263)$	0.8817
5	Color	$E_{27}(263)$	0.8138
5	Brand	$E_{27}(263)$	0.8817
10	Color	$E_{27}(263)$	0.8138
10	Brand	$E_{27}(263)$	0.8817
20	Color	$E_{27}(263)$	0.8138
20	Brand	$E_{27}(263)$	0.8817

Table 6: Impact of sampled image quantity on target embedding chosen and corresponding clustering performance across different criteria.

We conducted experiments on the Stanford_Cars dataset, evaluating the NMI score as the primary performance metric. We varied the number of sampled images per feature, testing configurations of [3, 5, 10, 20] examples, as illustrated in 6. We also compared the keyword generation capabilities of three distinct LLMs: GPT-4, DeepSeek-R1 (Guo et al. 2025), and Gemini-2.5 (Comanici et al. 2025), as shown in Table 7. For each test, target embeddings were derived using the prompting strategies detailed in Section 3.2. Our experiments confirm the robustness and high accuracy

LLM	Criterion	LLM Keyword Output	Target Embedding	Final NMI
GPT-4	Color	Black, White, Silver, Gray, Red, Blue, Green, Gold, Brown, Beige	$E_{27}(263)$	0.8138
	Brand	Toyota, Ford, Chevrolet, Honda, Nissan, Volkswagen, Hyundai, Mercedes-Benz, BMW, Audi	$E_{27}(263)$	0.8817
DeepSeek-R1	Color	White Black Gray Silver Red Blue Green Yellow Orange Brown Gold Beige Bronze Purple Pink	$E_{27}(263)$	0.8138
	Brand	Toyota Honda Ford Chevrolet Volkswagen BMW Mercedes Audi Nissan Hyundai Kia Tesla	$E_{27}(263)$	0.8817
Gemini-2.5	Color	White Black Grey Silver Blue Red Green Yellow Brown Beige Purple Gold	$E_{27}(263)$	0.8138
	Brand	Toyota Volkswagen Hyundai Kia Ford Honda Nissan Chevrolet BMW Mercedes	$E_{27}(263)$	0.8817

Table 7: Impact of LLM choice on keyword generation, target embedding and clustering performance. The LLMs are prompted with the input: "What are common car colors(brands)? Provide the answer with single words." The sample size for each feature is 10.

of our method across varied sampled image quantities and Large Language Model (LLM) choices for keyword generation. Despite this inherent stability, we recommend a sample size of 10-20 images per feature. This suggestion addresses scenarios where generated keywords might not overlap with the ground truth labels, necessitating manual verification of keywords obtained from the LLaVA's output.